

Tomography of the Quark-Gluon-Plasma by Charm Quarks

Taesoo Song,^{1,2,*} Hamza Berrehrah,^{1,2} Daniel Cabrera,^{1,2} Juan M. Torres-Rincon,³ Laura Tolos,^{2,4} Wolfgang Cassing,⁵ and Elena Bratkovskaya^{1,2}

¹*Institute for Theoretical Physics, Johann Wolfgang Goethe Universität, Frankfurt am Main, Germany*

²*Frankfurt Institute for Advanced Studies, Johann Wolfgang Goethe Universität, Frankfurt am Main, Germany*

³*Subatech, UMR 6457, IN2P3/CNRS, Université de Nantes,*

École des Mines de Nantes, 4 rue Alfred Kastler, 44307 Nantes cedex 3, France

⁴*Institut de Ciències de l'Espai (IEEC/CSIC), Campus Universitat Autònoma de Barcelona,*

Carrer de Can Magrans, s/n, E-08193 Bellaterra, Spain

⁵*Institut für Theoretische Physik, Universität Gießen, Germany*

We study charm production in ultra-relativistic heavy-ion collisions by using the Parton-Hadron-String Dynamics (PHSD) transport approach. The initial charm quarks are produced by the Pythia event generator tuned to fit the transverse momentum spectrum and rapidity distribution of charm quarks from Fixed-Order Next-to-Leading Logarithm (FONLL) calculations. The produced charm quarks scatter in the quark-gluon plasma (QGP) with the off-shell partons whose masses and widths are given by the Dynamical Quasi-Particle Model (DQPM), which reproduces the lattice QCD equation-of-state in thermal equilibrium. The relevant cross sections are calculated in a consistent way by employing the effective propagators and couplings from the DQPM. Close to the critical energy density of the phase transition, the charm quarks are hadronized into D mesons through coalescence and fragmentation. The hadronized D mesons then interact with the various hadrons in the hadronic phase with cross sections calculated in an effective lagrangian approach with heavy-quark spin symmetry. Finally, the nuclear modification factor R_{AA} and the elliptic flow v_2 of D^0 mesons from PHSD are compared with the experimental data from the STAR Collaboration for Au+Au collisions at $\sqrt{s_{NN}}=200$ GeV. We find that in the PHSD the energy loss of D mesons at high p_T can be dominantly attributed to partonic scattering while the actual shape of R_{AA} versus p_T reflects the heavy-quark hadronization scenario, i.e. coalescence versus fragmentation. Also the hadronic rescattering is important for the R_{AA} at low p_T and enhances the D -meson elliptic flow v_2 .

PACS numbers: 25.75.Nq, 25.75.Ld

I. INTRODUCTION

According to the fundamental theory of strong interactions, the Quantum Chromo Dynamics (QCD) [1], matter changes its phase at high temperature and density and bound (colorless) hadrons dissolve to interacting (colored) quarks and gluons – Quark-Gluon-Plasma (QGP). Such extreme conditions have existed in the early expansion of the universe and now can be realized in the laboratory by collisions of heavy-ions at ultra-relativistic energies. The study of the phase boundary and the properties of the QGP are the main goal of several present and future heavy-ion experiments at SPS (Super Proton Synchrotron), RHIC (Relativistic Heavy-Ion Collider), LHC (Large Hadron Collider) and the future FAIR (Facility for Antiproton and Ion Research) and NICA (Nuclotron-based Ion Collider fAcility) [2]. Since the QGP is created only for a short time (of a couple of fm/c) it is quite challenging to study its properties and to find the most sensible probes. In order to study the full complexity of the underlying problem, one needs to obtain comprehensive information by the measurement of the 'bulk' light hadrons, electromagnetic probes (dileptons

and photons), heavy mesons and jets. The advantage of the 'hard probes' such as the mesons containing heavy quarks (charm and beauty) is, firstly, that due to the heavy masses they are dominantly produced in the very early stages of the reactions with large energy-momentum transfer, contrary to the light hadrons and electromagnetic probes. Secondly, they are not in an equilibrium with the surrounding matter due to smaller interaction cross sections relative to the light quarks and, thus, may provide an information on their creation mechanisms. Moreover, due to the hard scale, perturbative QCD (pQCD) should be applicable for the calculation of heavy quark production. As shown in Ref. [3], the FONLL calculations are in good agreement with the experimental observables on charm meson spectra in p+p collisions. This provides a solid reference frame for studying the heavy-meson production in heavy-ion collisions.

The collective properties of open charm mesons have been addressed experimentally by measuring the nuclear modification factor R_{AA} , which is the ratio of the transverse momentum distribution in $A+A$ collisions relative to p+p collisions scaled by the number of binary collisions, as well as the collective elliptic flow v_2 . These two observables are comprehensive since the high p_T part of R_{AA} is very sensitive to the energy loss of charm quarks (or mesons) during their propagation through the partonic (or hadronic) medium due to the interac-

*Electronic address: song@fias.uni-frankfurt.de

tion processes. The low p_T part is more sensitive to the hadronization mechanism and, thus, provides constraints on the relative scale for the transition from partonic to hadronic degrees-of-freedom. Moreover, the elliptic flow v_2 of charm quarks characterizes the collectivity of the system developed from the very early stage to the freeze-out time thereby including interactions from the partonic and hadronic phase. Thus, the final momentum distribution of the heavy mesons is sensitive to the details of the expansion of the plasma itself as well as to the strength of the interaction of the heavy quark with the partons and the formed D -mesons with the hadronic environment. It depends on the density of partons (and their properties) present in the QGP and hence on whether the plasma is in equilibrium during the expansion.

The first charm measurements at RHIC energies by the PHENIX[4] and STAR [5] collaborations were related to the single non-photonic electrons emitted from the decay of charm mesons. However, recently the STAR Collaboration measured directly the nuclear modification factor and the elliptic flow of D^0 mesons in Au+Au collisions at $\sqrt{s_{NN}}=200$ GeV [6, 7] which allows for a straight forward comparison with the theoretical model calculations. It has been observed that the R_{AA} and v_2 of charm mesons show a similar behavior as in case of light hadrons contrary to expectations from pQCD. Similar observations have been made at LHC energies, too [8].

It still remains a challenge for the theory to reproduce the experimental data and to explain simultaneously the large energy loss of charm quarks (R_{AA}) and the strong collectivity (v_2) – cf. e.g. Refs. [9–25]. The interactions of charm quarks with the partonic medium are commonly based on pQCD with massless light quarks and a fixed or running coupling. The time evolution of the charm-quark distribution in the expanding fireball is approximated by the Fokker-Planck equation where the response of the partonic (or hadronic) medium is expressed in terms of temperature- and momentum-dependent drag and diffusion coefficients. The modeling of the temperature profile is often done in a fireball model or by hydrodynamic calculations (ideal or viscous) which start with some initial conditions and follow the dynamical evolution according to the chosen Equation-of-State (EoS) under the assumption of local equilibrium. In partonic cascade models one solves the Boltzmann equation for massless quarks/gluons with the pQCD cross sections for some fixed coupling α_s . The hadronization of charm quarks is done assuming coalescence at low p_T and fragmentation at high p_T . In spite that many models may describe the R_{AA} , it is still difficult to obtain simultaneously a consistent description of the elliptic flow v_2 using the same assumptions and model parameters [25], e.g. the choice of the running coupling, the K-factor to scale the pQCD cross sections, the time evolution profile, etc. Moreover, the conclusions on the amount of suppression due to collisional energy loss by means of the elastic interactions of charm quarks with the QGP partons versus the radiative energy loss due to the emission of soft gluons (i.e. gluon

bremsstrahlung) are still far from being robust. Also the influence of hadronization and especially hadronic rescattering is not yet settled, too. Moreover, the results turned out to be also sensitive to the time evolution models involved.

Our goal here is to study the charm dynamics based on a consistent microscopic transport approach for the charm production, hadronization and rescattering with the partonic and hadronic medium. In this study we will confront our calculations within the Parton-Hadron-String Dynamics (PHSD) approach to the experimental data on charm at RHIC energies and discuss the perspectives/problems of using the charm quarks for the tomography of the QGP. To achieve this goal we embed the heavy-quark physics in the existing PHSD transport approach [26] which incorporates explicit partonic degrees-of-freedom in terms of strongly interacting quasiparticles (quarks and gluons) in line with an equation-of-state from lattice QCD (lQCD) as well as dynamical hadronization and hadronic elastic and inelastic collisions in the final reaction phase. Since PHSD has been successfully applied to describe the final distribution of mesons (with light quark content) from lower SPS up to LHC energies [26–29], it provides a solid framework for the description of the creation, expansion and hadronization of the QGP as well as the hadronic expansion with which the heavy quarks interact either as quarks or as bound states such as D -mesons.

Thus, the principle differences of our approach to the previous dynamical models (including earlier HSD [30] studies on the charm dynamics [31]) are:

- (i) the degrees-of-freedom for the QGP are massive and strongly interacting quasiparticles contrary to massless and weakly interacting pQCD partons;
- (ii) a non-equilibrium off-shell microscopic transport approach is employed for the QGP dynamics, hadronization and the hadronic phase instead of simplified descriptions of the parton dynamics in terms of Fokker-Planck equations + QGP hydrodynamics (assuming local equilibration) or Boltzmann-type partonic cascades with massless light quarks;
- (iii) rescattering of D -mesons in the hadronic phase in line with an up-to-date effective Lagrangian approach from Ref. [32].

This paper is organized as follows: In Sec. II we recall the basic ideas of the PHSD approach while in Sec. III we describe the production of initial charm quark pairs in hard binary nucleon-nucleon collisions and their implementation in PHSD. In Sec. IV we present the interactions of charm quarks with off-shell partons in the QGP calculated earlier in Refs. [33–35], the hadronization of charm quarks in Sec. V, and the D meson interactions with hadrons in Sec. VI that are based on the cross sections from Ref. [32]. Finally, the nuclear modi-

fication factor R_{AA} and the elliptic flow v_2 of D mesons from PHSD are presented in Sec. VII and compared to the available data. A summary completes this work in Sec. VIII.

II. THE PHSD TRANSPORT APPROACH

The Parton-Hadron-String Dynamics (PHSD) transport approach [26, 27] is a microscopic covariant dynamical model for strongly interacting systems formulated on the basis of Kadanoff-Baym equations [36, 37] for Green's functions in phase-space representation (in first order gradient expansion beyond the quasiparticle approximation). The approach consistently describes the full evolution of a relativistic heavy-ion collision from the initial hard scatterings and string formation through the dynamical deconfinement phase transition to the strongly-interacting quark-gluon plasma (sQGP) as well as hadronization and the subsequent interactions in the expanding hadronic phase as in the Hadron-String-Dynamics (HSD) transport approach [30]. The transport theoretical description of quarks and gluons in the PHSD is based on the Dynamical Quasi-Particle Model (DQPM) for partons that is constructed to reproduce lQCD results for a quark-gluon plasma in thermodynamic equilibrium [38] on the basis of effective propagators for quarks and gluons. The DQPM is thermodynamically consistent and the effective parton propagators incorporate finite masses (scalar mean-fields) for gluons/quarks as well as a finite width that describes the medium dependent reaction rate. For fixed thermodynamic parameters (T, μ_q) the partonic widths $\Gamma_i(T, \mu_q)$ fix the effective two-body interactions that are presently implemented in the PHSD [39]. The PHSD differs from conventional Boltzmann approaches in a couple of essential aspects: i) it incorporates dynamical quasi-particles due to the finite width of the spectral functions (imaginary part of the propagators); ii) it involves scalar mean-fields that substantially drive the collective flow in the partonic phase; iii) it is based on a realistic equation of state from lattice QCD and thus describes the speed of sound $c_s(T)$ reliably; iv) the hadronization is described by the fusion of off-shell partons to off-shell hadronic states (resonances or strings) and does not violate the second law of thermodynamics; v) all conservation laws (energy-momentum, flavor currents etc.) are fulfilled in the hadronization contrary to coalescence models; vi) the effective partonic cross sections no longer are given by pQCD and are 'defined' by the DQPM in a consistent fashion and probed by transport coefficients (correlators) in thermodynamic equilibrium by performing PHSD calculations in a finite box with periodic boundary conditions (shear- and bulk viscosity, electric conductivity, magnetic susceptibility etc. [40, 41]).

In the beginning of relativistic heavy-ion collisions color-neutral strings (described by the FRITIOF LUND model [42]) are produced in hard scatterings of nucle-

ons from the impinging nuclei. These strings are dissolved into 'pre-hadrons' with a formation time of ~ 0.8 fm/c in their rest frame, except for the 'leading hadrons', i.e. the fastest residues of the string ends, which can re-interact (practically instantly) with hadrons with a reduced cross sections in line with quark counting rules. If, however, the local energy density is larger than the critical value for the phase transition, which is taken to be ~ 0.5 GeV/fm³, the pre-hadrons melt into (colored) effective quarks and antiquarks in their self generated repulsive mean-field as defined by the DQPM [38]. In the DQPM the quarks, antiquarks and gluons are dressed quasiparticles and have temperature-dependent effective masses and widths which have been fitted to lattice thermal quantities such as energy density, pressure and entropy density. The nonzero width of the quasiparticles implies the off-shellness of partons, which is taken into account in the scattering and propagation of partons in the QGP on the same footing (i.e. propagators and couplings). We point out that the DQPM does not provide effective propagators for the c - and \bar{c} -quarks since the latter degrees-of-freedom are subdominant in the entropy density for temperatures of 1 - 3 T_c due to their large mass and thus cannot be determined properly by the entropy from the lattice. Nevertheless, the interactions of the charm quarks with the light (u, d, s) quarks can be computed on the basis of the running coupling $g^2(T/T_c)$ in the DQPM and the effective propagators for the light quarks. As demonstrated in Ref. [33] the resulting differential cross sections of c, \bar{c} quarks only very slightly depend on the spectral width of the charm quarks such that even the on-shell limit for these degrees-of-freedom with a mass of ~ 1.5 GeV provides a very reasonable approximation [33, 34].

The transition from the partonic to hadronic degrees-of-freedom (for light quarks/antiquarks) is described by covariant transition rates for the fusion of quark-antiquark pairs to mesonic resonances or three quarks (antiquarks) to baryonic states, i.e. by the dynamical hadronization. We already mention here that this hadronization process is restricted to 'bulk' transverse momenta p_T up to ~ 2 GeV and has to be replaced by fragmentation for high p_T . Note that due to the off-shell nature of both partons and hadrons, the hadronization process described above obeys all conservation laws (i.e. four-momentum conservation and flavor current conservation) in each event, the detailed balance relations and the increase in the total entropy S . In the hadronic phase PHSD is equivalent to the hadron-strings dynamics (HSD) model [30] that has been employed in the past from SchwerIonen-Synchrotron (SIS) to SPS energies. On the other hand the PHSD approach has been applied to p+p, p+A and relativistic heavy-ion collisions from lower SPS to LHC energies and been successful in describing a large number of experimental data including single-particle spectra, collective flow as well as electromagnetic probes [26–29].

In this study we use the Pythia event generator [43]

for nucleon-nucleon binary collisions to produce charm-quark pairs in relativistic heavy-ion collisions and evolve the dynamics of the charm quarks within PHSD in order to understand the dominant mechanisms in comparison to the recent experimental data on D^0 mesons from STAR. Whereas the dynamics of the charm quarks is essentially Boltzmann-like, i.e. without mean-fields and dynamical width, their interactions with the dynamical partons (light quarks and gluons) is based on the effective coupling from the DQPM and the DQPM propagators [33, 34].

III. INITIAL CHARM QUARK PRODUCTION

Before studying the charm production in relativistic heavy-ion collisions, we discuss the charm production in p+p collisions at the top RHIC energy of $\sqrt{s_{NN}} = 200$ GeV. The charm production in p+p collisions also plays the role as a reference for the nuclear modification factor R_{AA} in heavy-ion collisions.

We use the Pythia event generator to produce charm and anticharm quarks in p+p collisions with the parameters $PARP(91)=1.0$ GeV/c and $PARP(67)=1.0$ as in Ref. [43, 44]. The former parameter is the Gaussian width of the primordial transverse momentum of a parton which initiates a shower in hadrons and the latter the parton shower level parameter. We note that by an additional suppression of the transverse momenta of charm and anticharm quarks by 10 % and a suppression of rapidities by 16 % the transverse momentum spectrum as well as rapidity distribution of charm and anticharm quarks from the Pythia event generator are very similar to those from the FONLL calculations in p+p collisions at $\sqrt{s_{NN}} = 200$ GeV as shown in Fig. 1. Here the red dot-dashed lines are from the Pythia event generator (after tuning) and the blue dotted lines from the FONLL calculations, respectively.

The produced charm and anticharm quarks hadronize by emitting soft gluons. The probabilities for a charm quark to hadronize into D^0 , D^+ , D^{*0} , D^{*+} , D_s^+ , and Λ_c are, respectively, taken to be 0.2, 0.174, 0.213, 0.224, 0.08, and 0.094 [45]. The momentum of the hadronized D meson or Λ_c is given by the fragmentation function [46],

$$D_Q^H(z) \sim \frac{1}{z[1 - 1/z - \epsilon_Q/(1 - z)]^2}, \quad (1)$$

where z is the momentum fraction of the hadron H fragmented from the heavy quark Q while ϵ_Q is a fitting parameter which is taken to be $\epsilon_Q = 0.01$ in our study. We note that the parameter ϵ_Q used here is smaller than the usual value because the transverse momentum of charm quarks is reduced in our study. The solid line in Fig. 1 (upper part) shows the transverse momentum spectrum of D^0 mesons after charm quark fragmentation including the contribution from the decay of D^{*0} and D^{*+} . We

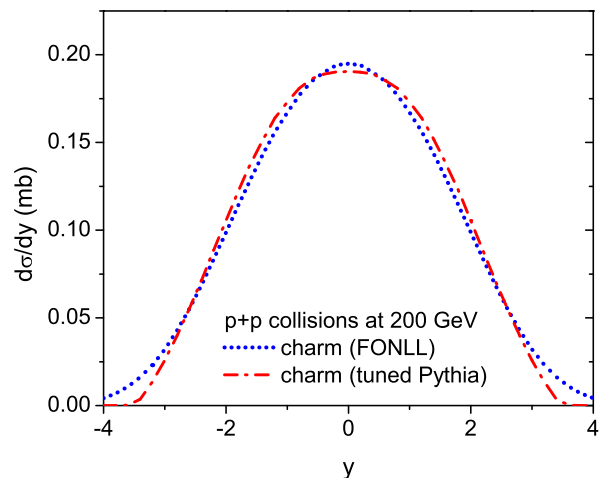
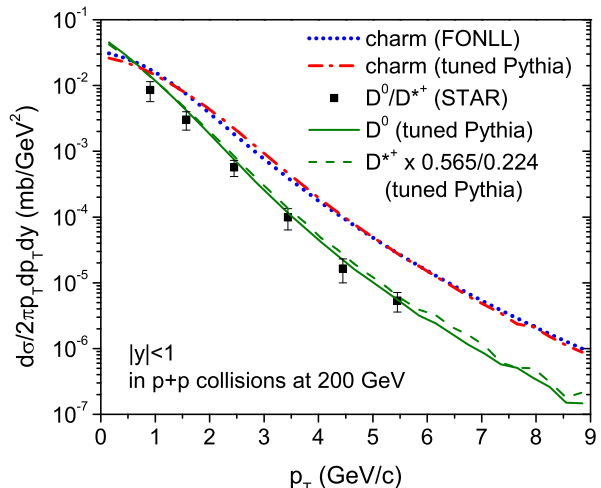


FIG. 1: (Color online) Transverse momentum (upper) and rapidity (lower) distributions of charm quarks in p+p collisions at $\sqrt{s_{NN}} = 200$ GeV from FONLL (dotted lines) and the tuned Pythia event generator (dot-dashed lines); in the upper part the transverse momentum spectrum of D^0 mesons which are fragmented from charm quarks with the contribution from D^* decay included (solid line) and that of D^{*+} after scaling are compared with the experimental data from the STAR Collaboration [44].

can see that our results reproduce the experimental data from the STAR Collaboration [44] reasonably well.

In heavy-ion collisions, the nucleons in the target and projectile nuclei are distributed in coordinate space according to the nuclear density distribution given by

$$\rho(r) \sim \frac{1}{1 + \exp[(r - r_0)/a]}, \quad (2)$$

where $r_0 = 1.124A^{1/3}$ and $a = 0.02444A^{1/3} + 0.2864$ with A being the mass number of the target or projectile nucleus. Each nucleon has Fermi motion depending on the

local nucleon density which is chosen randomly by Monte Carlo. Although the Fermi momentum is small in the rest frame of each nucleus, the component along the beam direction becomes large in the laboratory frame due to the Lorentz transformation ($\gamma_{cm} \approx 100$ at the top RHIC energy). Accordingly, the Fermi motions smears the energy of nucleon-nucleon binary collisions in relativistic heavy-ion collisions. The lower part of Fig. 2 shows the distribution of binary nucleon-nucleon collision energies in 0-10 % central Au+Au collisions at $\sqrt{s_{NN}} = 200$ GeV from PHSD. We mention that this Fermi smearing is usually neglected in theoretical models for charm production and propagation which is not crucial at RHIC energies but becomes important close to threshold energies for charm production.

Since charm-quark production requires a high energy-momentum transfer, the number of produced charm quark pairs in relativistic heavy-ion collisions is proportional to the number of binary nucleon-nucleon collisions N_{bin} . Since the probability to produce a charm quark pair depends on invariant energy and is less than that for primary hard collision in the PHSD, the binary nucleon-nucleon collisions producing charm quark pairs are chosen by Monte Carlo from the ratio of the cross section for charm production in nucleon-nucleon collision, $\sigma_{cc}^{pp}(\sqrt{s})$, to the inelastic nucleon-nucleon cross section. The total cross section in PHSD for charm production in nucleon-nucleon collisions is parameterized by

$$\sigma_{cc}^{pp}(\sqrt{s}) = A[1 - \sqrt{(s_0/s)}]^\alpha (s/s_0)^\beta, \quad (3)$$

where A , α and β are fit parameters. We use two different parameter sets, one for $\sqrt{s} \leq 200$ GeV and the other for $\sqrt{s} > 200$ GeV to fit the experimental data covering a wide range of collision energies as shown in the upper part of Fig. 2; both parameterizations are smoothly connected at $\sqrt{s} = 200$ GeV.

The energy-momenta of the produced charm and anticharm quarks in each collision event are given by the Pythia event generator as in p+p collisions but for the actual (smeared) collision energy. In the Pythia event generator, the charm and anticharm quarks are produced in the center-of-mass frame of two colliding nucleons with the incident nucleons being aligned along the z -direction. Therefore in PHSD we rotate the momenta of the generated charm and anticharm quark to the original orientation of the two incident nucleons in their center-of-mass frame and then boost to the calculational frame. We assume that the two nucleons, which produce the charm quark pair, keep their transverse momentum and lose only longitudinal momentum such that the total energy (including the produced charm quark pair) is conserved and the two nucleons are still on-shell after the hard collision. Although this prescription seems to violate spatial momentum conservation, we have to mention that this violation is very small since the charm quark pair is produced together with several (plenty) light hadrons in the same event which balance the spatial momentum.

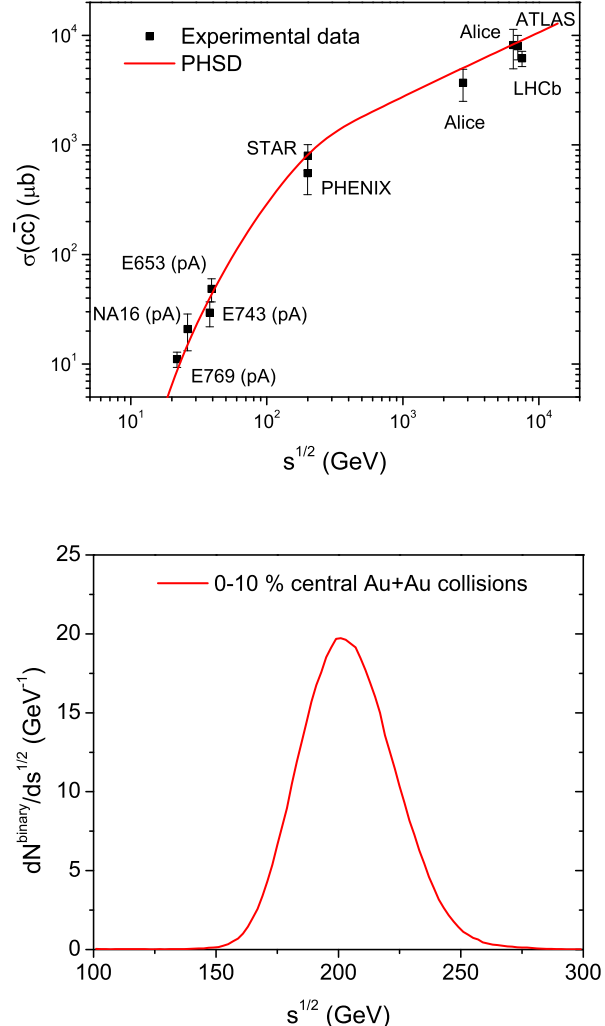


FIG. 2: (Color online) The total cross section for charm production in p+p collisions (as parameterized in the PHSD) is compared with the experimental data at various collision energies [44, 47] (upper panel); the distribution of binary nucleon-nucleon collision energies in 0-10 % central Au+Au collisions at $\sqrt{s_{NN}} = 200$ GeV from PHSD including Fermi smearing (lower panel).

IV. CHARM-QUARK SCATTERING IN THE QGP

A. $q + c$ and $g + c$ elastic scattering cross sections

Quarks, antiquarks, and gluons are dressed in the QGP and have temperature-dependent effective masses and widths. In the DQPM, the mass and width of the light partons are given by thermal quantum-field theory assuming leading order diagrams but the strong coupling $g^2(T)$ is fitted to lattice data on energy and entropy densities, etc. [38]. Note that a nonzero width of a parton

reflects the off-shell nature as well as the strong interaction of the quasi-particle and finite life-time.

The charm and anticharm quarks produced in early hard collisions interact with the dressed off-shell partons in the QGP. The cross sections for the charm quark scattering with massive off-shell partons are calculated considering the mass spectra of final state particles [33, 34]. In the current study the charm quark mass is taken to be 1.5 GeV and its mass spectrum is neglected for simplicity. Since the charm quark is heavy, the off-shell effect is small contrary to the light quarks and gluons (see Refs. [33, 34] for a quantitative study of this effect). Moreover, the off-shell effects from parton spectral functions are small, except for reducing the kinematic threshold.

In the current study we consider only elastic scattering of charm quarks by light quarks and gluons. We do not consider yet the radiative processes which generate radiative energy loss because we expect that, due to the large gluon mass in the DQPM, the radiative processes are sub-dominant as compared to the collisional ones, especially for low charm-quark momenta (p_T). We expect the radiative energy loss to contribute at very high p_T as accessible experimentally at the LHC [48].

The elastic scattering of charm quarks in the QGP is treated in our study by including the non-perturbative effects of the strongly interacting quark-gluon plasma (sQGP) constituents, i.e. the large coupling, the multiple scattering etc. The multiple strong interactions of quarks and gluons in the sQGP are encoded in their effective propagators with broad spectral functions. As pointed out above the effective propagators, which can be interpreted as resummed propagators in a hot and dense QCD environment, have been extracted from lattice data in the scope of the DQPM [38]. Furthermore, in Refs. [33, 34] we have evaluated, to the lowest order in the perturbation expansion, the transition amplitudes of the processes $q + c \rightarrow q + c$ and $g + c \rightarrow g + c$ as shown in Fig. 3. Contrary to the case of massless gluons where the ‘‘Transverse gauge’’ is used, we use the ‘‘Lorentz covariance’’ for the case of massive gluons since a finite mass in the gluon propagator allows to fix the 0-th components of the gluon fields $A_a^0 (a = 1; \dots; 8)$ by the spatial degrees of freedom $A_a^k (k = 1; 2; 3)$. Furthermore, the divergence encountered in the t -channel when calculating the total cross sections (σ^{qc}) and (σ^{gc}) is cured self-consistently in our computation since the infrared regulator is given by the finite DQPM gluon mass (and width).

For the scattering of charm quark by the light quark and gluon with finite masses and widths, we take into account the spectral functions of the light quark and gluon, and the temperature-dependent running coupling, $g^2(T)$. The propagators of massive vector gluons with finite life-time and of charm quark with zero life time are, respectively, given by

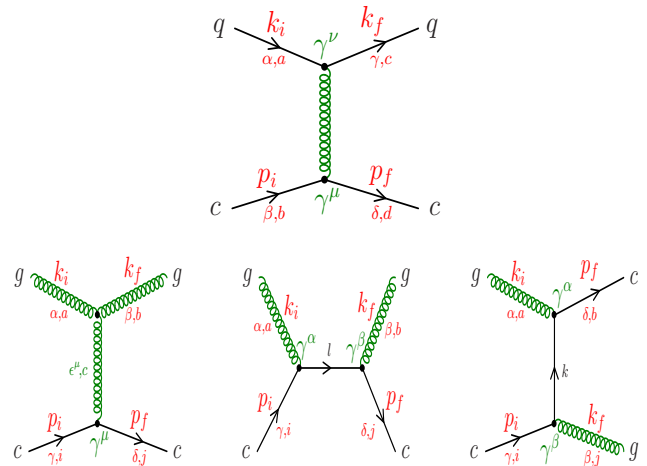


FIG. 3: (Color online) Feynman diagrams for the scattering of $q + c \rightarrow q + c$ and $g + c \rightarrow g + c$. Latin (Greek) subscripts denote colour (spin) indices. k_i and p_i (k_f and p_f) denote the initial (final) 4-momentum of the light quark or the gluon and the heavy quark, respectively.

$$G^{\mu\nu}(q) = -i \frac{g^{\mu\nu} - q^\mu q^\nu / m_g^2}{q^2 - m_g^2 + i2\gamma_g q_0},$$

$$S(p) = \frac{\not{p} + m_c}{p^2 - m_c^2}, \quad (4)$$

where m_g , γ_g are, respectively, gluon mass and width at finite temperature, and the charm quark mass m_c is taken to be 1.5 GeV.

Fig. 4 shows the elastic cross section of an on-shell charm quark with off-shell u -quarks (σ^{uc}) as a function of the temperature and \sqrt{s} , the energy available in the center-of-mass frame. Apart from the threshold region the cross section is rather independent of \sqrt{s} , and decreases with increasing temperature mainly due to a smaller coupling strength at high temperature. The large cross section near the critical temperature $T_c = 0.158$ GeV is related to the infrared enhancement of the coupling $\alpha_s(T)$ in the DQPM. The cross section for charm quark and gluon elastic scattering is about twice (9/4 which is the ratio of the different color Casimir operators squared) that for charm quark and light quark scattering.

Our cross sections also depend on the scattering angle besides collision energy \sqrt{s} and temperature T . Fig. 5 presents the differential cross sections $d\sigma/d\cos\theta$ for on-shell charm quark scattering with off-shell u -quarks at $\sqrt{s} = 3$ GeV (orange lines) and 4 GeV (black lines) for temperatures of $1.2 T_c$, $2 T_c$ and $3 T_c$. Different from the pQCD-inspired models, $d\sigma/d\cos\theta$ in our ‘non-perturbative’ model is not so much forward peaked (large enhancement for small angles or small momentum transfers t) [33]. Therefore, efficient momentum transfers more often occur in our partonic scattering as compared to the usual pQCD $2 \rightarrow 2$ scattering [34].

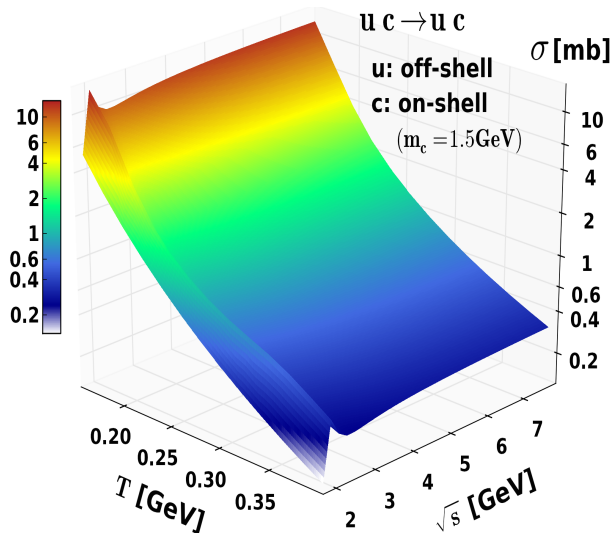


FIG. 4: (Color online) Elastic cross section for $u + c \rightarrow u + c$ scattering as a function of the temperature T and the invariant energy \sqrt{s} where the u -quark is off-shell and the charm quark has a constant mass of 1.5 GeV [33, 34].

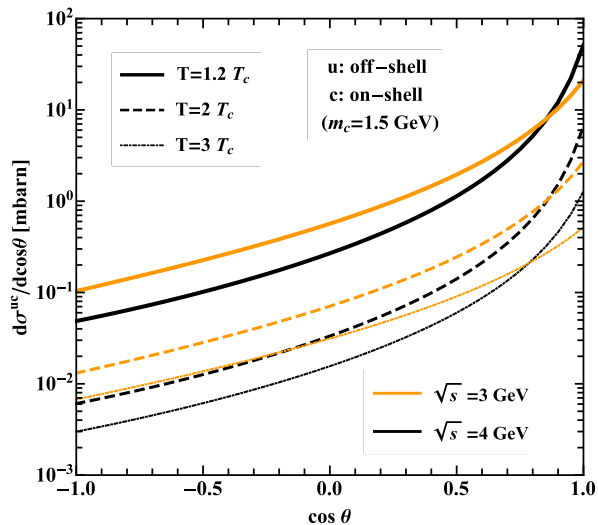


FIG. 5: (Color online) Differential elastic cross section for the scattering of an on-shell charm quark and off-shell u -quarks at $\sqrt{s} = 3$ GeV (orange lines) and 4 GeV (black lines) for temperatures of $1.2 T_c$, $2 T_c$ and $3 T_c$, with $T_c = 0.158$ GeV. We take 1.5 GeV for the charm quark mass and DQPM spectral functions (propagators) for the light off-shell partonic degrees-of-freedom [33].

B. Charm spatial diffusion coefficient

Using the transition amplitudes for the elastic scattering of charm quarks by the partons in medium, one can calculate the charm spatial diffusion coefficient D_s from

the drag coefficient, $A = \frac{d\langle \mathbf{p}_c \rangle}{dt}$ through $\eta_D = A/p_c$:

$$D_s = \lim_{p_c \rightarrow 0} \frac{T}{m_c \eta_D}, \quad (5)$$

or from the diffusion coefficient $\kappa = \frac{1}{3} \frac{d\langle (\mathbf{p}_c - \mathbf{p}'_c)^2 \rangle}{dt}$:

$$D_s = \lim_{p_c \rightarrow 0} \frac{\kappa}{2m_c^2 \eta_D^2}. \quad (6)$$

Both definitions agree with each other if the Einstein relation is valid [34, 35].

Using Eq. (6), we show in Fig.6 the spatial diffusion coefficient D_s as a function of T for $\mu_q = 0$. Our results are compared to the lattice calculations, which have recently been confirmed by the Bielefeld collaboration [49], for temperatures above $T_c \approx 160$ MeV and with the spatial diffusion coefficient of a heavy meson in hadronic matter [32] for temperatures below 180 MeV. We observe that the spatial diffusion coefficients in hadronic and partonic matters meet each other and have a pronounced minimum around T_c . Fig. 6 shows that our results agree with those from the lattice QCD. The smooth transition of the heavy-quark transport coefficients from the hadronic to the partonic medium corresponds to a crossover in line with lattice calculations, and differs substantially from perturbative QCD (pQCD) calculations which show a large discontinuity of D_s close to T_c [34, 35].

We emphasize that the transport coefficient D_s extracted from our microscopic calculations and its agreement with the lQCD results (within errors) and the corresponding D meson D_s in hadronic medium validate our description for the coupling of charm with the QGP matter.

Fig. 7 shows the distributions of charm and anticharm quark scattering with quarks/antiquarks (solid line) and gluons (dashed line) as a function of the invariant energy \sqrt{s} in 0-10 % central Au+Au collisions. The total number of charm and anticharm quark scatterings with light quarks and light antiquarks is about 135 and that with gluons is about 83. We recall that about 19 pairs of charm and anticharm quarks are produced in this centrality range; each charm or anticharm quark thus experiences on average 6 elastic scatterings with partons before it is hadronized. Since the dressed quark/antiquark mass is smaller than the dressed gluon mass, the peak of the distribution for charm and quark scattering is located at a lower energy compared to that of charm and gluon scattering. We additionally note that the number of charm quark scatterings with gluons is not small compared to that with quarks although the number of gluons is significantly smaller than that of quarks due to their larger mass. This is because the cross section for the charm and gluon elastic scattering is about twice that for charm and light quark elastic scattering. One characteristic of the partonic scattering of charm quarks is that the scattering distribution in \sqrt{s} has a long tail up to high invariant energies beyond that expected in a thermal equilibrium.

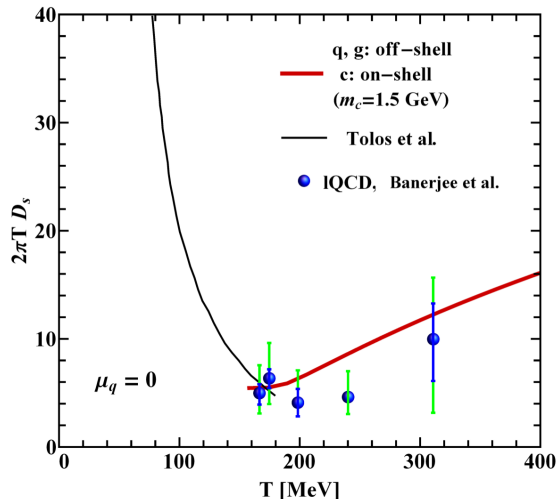


FIG. 6: (Color online) Spatial diffusion coefficient of heavy quark, D_s , as a function of T for $\mu_q = 0$. The black solid line below $T = 180$ MeV is the hadronic diffusion coefficient [32], and the red solid line above $T_c \approx 160$ MeV our D_s computation in the partonic environment. The lattice calculations are from Ref. [49].

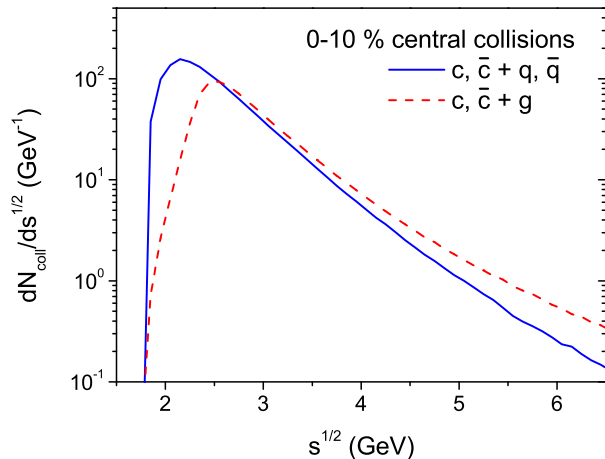


FIG. 7: (Color online) The distributions of charm and anticharm quark scattering by quarks/antiquarks (solid line) and gluons (dashed line) as a function of the invariant energy \sqrt{s} in 0-10% central Au+Au collisions.

This is attributed to the cross section for charm and parton elastic scattering which does not decrease with increasing \sqrt{s} as shown in Fig. 4. Therefore, the partonic scattering is effective for the energy loss of charm and anticharm quarks at high transverse momentum.

Fig. 8 compares the transverse-momentum spectrum of charm and anticharm quarks at the initial production with that at hadronization in the midrapidity interval ($|y| < 1$). We can see that the scattering with massive

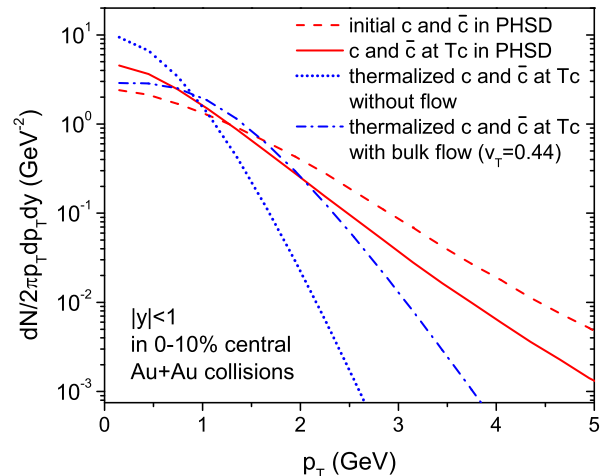


FIG. 8: (Color online) Transverse momentum spectra of charm and anticharm quarks at the initial production (dashed red line) and at hadronization (solid red line) in 0-10% central Au+Au collisions, compared with those of thermal charm quarks with (dot-dashed blue line) and without (dotted blue line) considering the transverse flow of the bulk particles at $T=158$ MeV which is the critical temperature for the QGP phase transition in PHSD.

partons softens the transverse momentum spectrum of charm quarks substantially. These spectra are also compared in Fig. 8 with the thermal spectrum of charm and anticharm quarks at T_c with the number of charm and anticharm quarks being the same as in the PHSD. The dot-dashed blue line in Fig. 8 shows the spectrum when we take into account the transverse flow velocity v_T of the bulk particles which is about 0.44 at T_c in 0-10% central collisions in the PHSD simulations:

$$\frac{dN}{2\pi p_T dp_T dy} \sim m_T I_0(\alpha) K_1(\beta), \quad (7)$$

where $m_T = \sqrt{m_c^2 + p_T^2}$, $\alpha = p_T \sinh \rho / T$ and $\beta = m_T \cosh \rho / T$ with $\rho = \tanh^{-1} v_T$, and K_1 and I_0 are modified Bessel functions [50].

The dotted blue line shows the spectrum without including the transverse flow ($v_T = 0$). Since the transverse flow velocity of charm quarks in relativistic heavy-ion collisions is smaller than that of the bulk particles, even though they are completely thermalized [51], the transverse-momentum spectrum of thermalized charm quarks is between the dotted blue and the dot-dashed blue lines. This figure suggests that charm and anticharm quarks are close to thermal equilibrium at low transverse momentum ($p_T < 2$ GeV) after partonic scattering while they are still off-equilibrium at higher transverse momenta since the solid red and the dot-dashed blue line start to deviate substantially for higher p_T .

V. HADRONIZATION OF CHARM QUARKS

Since the hot and dense matter created by a relativistic heavy-ion collision expands with time, the energy density of the matter decreases and the deconfined degrees-of-freedom hadronize to color neutral hadronic states. Once the local energy density in PHSD becomes lower than $0.5 \text{ GeV}/\text{fm}^3$, the partons are hadronized. First we look for all combinations of a charm quark and light antiquarks or of an anticharm quark and a light quark and calculate the probability for each combination to form a D or D^* (or D_s, D_s^*) meson. The probability for a quark and an anti-quark to form a meson is given by

$$f(\boldsymbol{\rho}, \mathbf{k}_\rho) = \frac{8g_M}{6^2} \exp \left[-\frac{\boldsymbol{\rho}^2}{\delta^2} - \mathbf{k}_\rho^2 \delta^2 \right], \quad (8)$$

where g_M is the degeneracy of the meson M , and

$$\boldsymbol{\rho} = \frac{1}{\sqrt{2}}(\mathbf{r}_1 - \mathbf{r}_2), \quad \mathbf{k}_\rho = \sqrt{2} \frac{m_2 \mathbf{k}_1 - m_1 \mathbf{k}_2}{m_1 + m_2}, \quad (9)$$

with m_i , \mathbf{r}_i and \mathbf{k}_i being the mass, position and momentum of the quark or antiquark i , respectively. The width parameter δ is related to the root-mean-square radius of the meson produced through

$$\langle r^2 \rangle = \frac{3}{2} \frac{m_1^2 + m_2^2}{(m_1 + m_2)^2} \delta^2 \quad (10)$$

and thus determined by experiment (if available).

The degeneracy factors, g_M , for D and D^* mesons are 1 and 3, respectively. We also take into account higher excited states of D mesons from the Particle Data Group [52]: $D_0^*(2400)^0$, $D_1(2420)^0$, and $D_2^*(2460)^{0,\pm}$. They dominantly decay into $D + \pi$ or $D^* + \pi$ and each branching ratio is not known yet. Therefore, we assume that the higher excited state decays immediately after hadronization into $D + \pi$ or $D^* + \pi$ with the branching ratio of 1 to 3, keeping its flavor. We further simplify that higher excited states have the same mass, 2460 MeV, since $D_2^*(2460)^{0,\pm}$ are most abundantly produced in the coalescence model due to its large spin, and they are assumed to have the same radius as D and D^* mesons.

In the actual simulations of the PHSD we perform several tens of events in parallel to obtain smooth local energy and particle number densities as a function of time; the charm or anticharm quark in the hadronization is allowed to take its partner from other events. Therefore, the coalescence probability given in Eq. (8) is divided by the number of parallel events such that the results become independent on the number of parallel runs.

Collecting all possible combinations of a charm or an anticharm quark with light quarks or antiquarks and calculating the coalescence probability for each combination from Eq. (8), we obtain the probability for the charm or the anticharm quark to hadronize by coalescence in the actual space-time volume $\Delta t \Delta x \Delta y \Delta z$. Whether the charm or the anticharm quark is actually hadronized by

coalescence is decided by Monte Carlo. Once the charm or the anticharm quark is decided to be hadronized by coalescence, then we find its partner again by Monte Carlo on the basis on the probability of each combination in the selected local ensemble. In case the charm or anticharm quark is decided not to hadronize by coalescence, it is hadronized by the fragmentation method as in p+p collisions (see Sec. III). Since the hadronization by coalescence is absent in p+p collisions, it can be interpreted as a nuclear matter effect on the hadronization of charm and anticharm quarks.

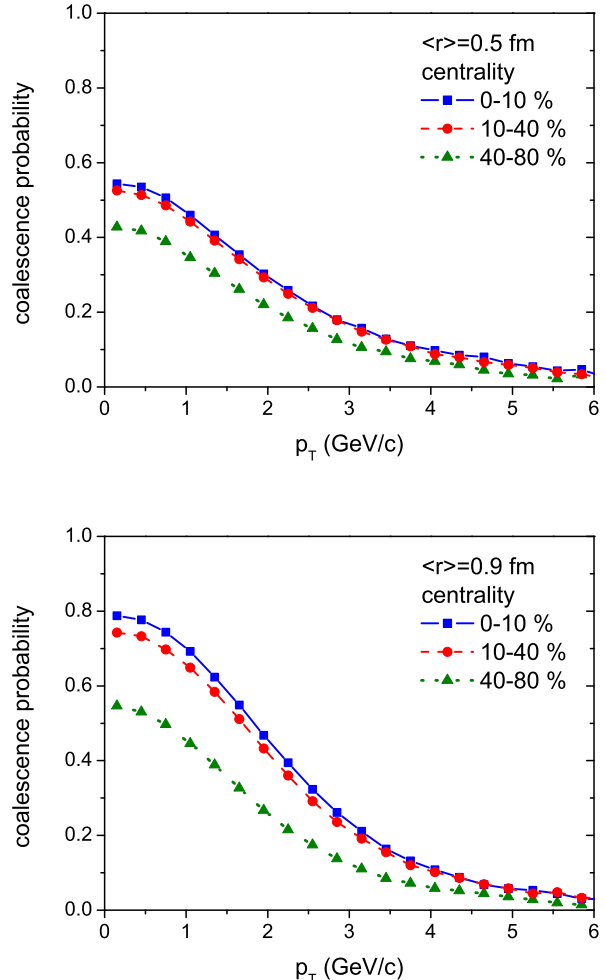


FIG. 9: (Color online) The probabilities for charm or anticharm quarks to hadronize to D or \bar{D} meson through coalescence as a function of transverse momentum in 0-10, 10-40, 40-80 % central Au+Au collisions at $\sqrt{s_{\text{NN}}} = 200 \text{ GeV}$ for the D meson radius of 0.5 fm (upper) and of 0.9 fm (lower).

Fig. 9 shows the probabilities for charm and anticharm quarks to hadronize to D and \bar{D} mesons through coalescence as a function of transverse momentum p_T in 0-10, 10-40, 40-80 % central Au+Au collisions at $\sqrt{s_{\text{NN}}} = 200 \text{ GeV}$ for the D meson radius of 0.5 fm (upper) and 0.9 fm

(lower). We can see that the probability decreases as the transverse momentum of the charm or anticharm quark increases. The reason is that the charm or anticharm quark with larger transverse momentum has less chance to find a neighboring coalescence partner in phase space.

Fig. 9 also shows that coalescence probability depends on centrality and the radius of the D meson. Since there are more light partons as a coalescence partner for the charm or anticharm quark in central collisions, the coalescence probability increases with decreasing centrality. In extremely peripheral collisions, however, the coalescence probability becomes tiny – as in p+p collisions – and the nuclear modification factor of D mesons naturally approaches to 1. Since the hadronization of charm quarks through fragmentation is not properly suited at low transverse momentum, several studies have forced the coalescence probability to be 1 at $p_T = 0$ [14, 17, 20, 53]. Unless only a single centrality is concerned, it is technically difficult to do so for all centralities by using the same coalescence parameters. Moreover, if the coalescence probability is 1 in peripheral collisions, it will induce a large nuclear modification factor, although small nuclear matter effect is expected in such collisions. Therefore, we allow the fragmentation of charm quarks at low transverse momentum as in p+p collisions in competition with coalescence (for different radii of the D -mesons). In Fig. 9 we see that the coalescence probability is larger for the D meson radius of 0.9 fm than of 0.5 fm. We note that while the smaller radius is more physical for D -mesons, a somewhat larger radius has been used in several studies [17, 53] to get a larger coalescence probability.

The energy-momentum difference between the charm or anticharm quark and the fragmented D or \bar{D} meson in fragmentation and the energy difference in coalescence are distributed equally to the surrounding partons (in the same cell) which are not hadronized yet to conserve the total energy-momentum of the system.

VI. D MESON SCATTERING IN THE HADRON GAS

The D and D^* mesons produced through coalescence or fragmentation interact with the surrounding hadrons in PHSD. The presence of several resonances close to threshold energies with dominant decay modes involving open-charm mesons and light hadrons suggests that the scattering cross sections of a D/D^* off a meson or baryon, highly abundant in the post-hadronization medium, could manifest a non-trivial energy, isospin and flavor dependence. An example of these states is the broad scalar resonance $D_0(2400)$, which decays into the pseudoscalar ground state D by emitting a pion in the s -wave (similarly to the heavy-quark spin partner

$D_1(2420)$, decaying into $D^*\pi^1$). Moreover, the similarity between the $\Lambda(1405)$ and the $\Lambda_c(2595)$ has driven the attention to the fact that the latter could be playing the role of a sub-threshold resonance in the DN system, connected to the latter by coupled-channel dynamics.

All these features have been addressed within several recent approaches based on hadronic effective models which incorporate chiral symmetry breaking in the light sector. The additional freedom stemming from the coupling to heavy-flavored mesons is constrained by imposing heavy-quark spin symmetry (HQSS) [32, 54–59]. Whereas chiral symmetry fully determines the scattering amplitudes of Goldstone bosons with other hadrons at leading order in a model independent way, by means of HQSS the dynamics of the pseudoscalar and the vector mesons containing heavy quarks can be connected, since all kinds of spin interactions are suppressed in the limit of infinite quark masses.

Following [54] (and references therein), the Lagrangian density describing the interaction between the spin-zero and spin-one D mesons with the light pseudoscalar (Goldstone) bosons from the octet (π, K, \bar{K}, η) reads $\mathcal{L} = \mathcal{L}_{\text{LO}} + \mathcal{L}_{\text{NLO}}$, where the subscripts LO and NLO refer to the leading and next-to-leading orders in the chiral perturbative expansion, whereas one keeps at leading order in the heavy-quark expansion. The LO Lagrangian reads

$$\begin{aligned} \mathcal{L}_{\text{LO}} = & \langle \nabla^\mu D \nabla_\mu D^\dagger \rangle - m_D^2 \langle DD^\dagger \rangle - \langle \nabla^\mu D^{*\nu} \nabla_\mu D_\nu^{*\dagger} \rangle \\ & + m_D^2 \langle D^{*\mu} D_\mu^{*\dagger} \rangle + ig \langle D^{*\mu} u_\mu D^\dagger - D u^\mu D_\mu^{*\dagger} \rangle \\ & + \frac{g}{2m_D} \langle D_\mu^* u_\alpha \nabla_\beta D_\nu^{*\dagger} - \nabla_\beta D_\mu^* u_\alpha D_\nu^{*\dagger} \rangle \epsilon^{\mu\nu\alpha\beta}, \end{aligned} \quad (11)$$

where $D = (D^0, D^+, D_s^+)$ and $D_\mu^* = (D^{*0}, D^{*+}, D_s^{*+})_\mu$ are the SU(3) antitriplets of spin-zero and spin-one D mesons, respectively, with mass m_D in the chiral limit, and the brackets denote the trace in flavor space. Two interaction terms are present in the LO Lagrangian, containing the coupling of the D and D^* meson fields to the light-meson axial vector current, $u_\mu = i(u^\dagger \partial_\mu u - u \partial_\mu u^\dagger)$, which describe, for instance, the decay of the D^* meson into a $D\pi$ pair. We note that the two terms are in principle independent but HQSS demands that both are related by a unique coupling constant g . The covariant derivative contains the coupling to the light-meson vector current and reads $\nabla_\mu = \partial_\mu - \frac{1}{2}(u^\dagger \partial_\mu u + u \partial_\mu u^\dagger)$, where the Goldstone bosons are introduced within the non-linear realization

¹ According to quark model predictions, the excitation spectrum of the D/D^* system consists of a triplet and a singlet of positive parity, with $J^P = 0^+, 1^+, 2^+$ and 1^+ , respectively (corresponding to ${}^{2S+1}L_J = {}^3P_J$ and 1P_1). The 1^+ states mix in such a way that the meson with the lower mass, $D_1(2420)$, becomes narrow and decouples from the $D^*\pi$ low-energy dynamics. The higher one, $D_1(2420)$, on the contrary, is very broad and decays predominantly in $D^*\pi$. The tensor state, $D_2^*(2460)$, is also narrow and its influence can be, in principle, disregarded.

of chiral symmetry in exponential parameterization, $U = u^2 = \exp\left(\frac{\sqrt{2}i\Phi}{f}\right)$, with

$$\Phi = \begin{pmatrix} \frac{1}{\sqrt{2}}\pi^0 + \frac{1}{\sqrt{6}}\eta & \pi^+ & K^+ \\ \pi^- & -\frac{1}{\sqrt{2}}\pi^0 + \frac{1}{\sqrt{6}}\eta & K^0 \\ K^- & \bar{K}^0 & -\frac{2}{\sqrt{6}}\eta \end{pmatrix} \quad (12)$$

and f the meson decay constant in the chiral limit ($f = 93$ MeV).

The NLO Lagrangian, which we omit here for simplicity, introduces twelve low-energy constants (LECs), h_i and \tilde{h}_i ($i = 0, \dots, 5$), which have to be fixed by symmetry arguments and known phenomenology. Imposing HQSS at LO reduces the number of free parameters to six, since $h_i = \tilde{h}_i$, whereas by large- N_c considerations it can be argued that only the odd LECs contribute.

The interaction of D mesons with baryons has been recently studied in different approaches which incorporate heavy flavor in the meson baryon interaction, either by implementing t -channel vector-meson exchange mechanisms between pseudoscalar mesons and baryons, by extending the Jülich meson-exchange model, or relying on the hidden gauge formalism (see [60] and references therein). Among these we recourse to the model described in Refs. [57–59, 61], which generalizes the Weinberg-Tomozawa form of the meson-baryon interaction, fixed by chiral symmetry at leading order, beyond flavor SU(3) structure. In addition, in this model HQSS is fulfilled exactly whenever charm quarks participate in the interaction. In all charm sectors, and in particular in $C = 1$ ($C =$ charm number), the theory accounts for point-like s -wave interactions between charmed mesons and light mesons in the pseudoscalar and vector octets, and the lowest lying baryons from the $J^P = 1/2^+$ (nucleon) octet and the $3/2^+$ (Delta) decuplet. It reduces to the WT interaction prescribed by chiral symmetry as long as the pseudoscalar mesons (Goldstone bosons) are involved. The latter is accomplished by enhancing the standard SU(3) flavor symmetry to a SU(6) spin-flavor symmetry [SU(8) when charm is also considered], which has allowed to identify unambiguously many baryonic states as dynamically generated resonances of the meson-baryon interaction in the light sector [57–59, 61]. HQSS imposes that arbitrary rotations of the heavy-quark spin should leave dynamics unchanged, which prevents charm flavor to be exchanged between the interacting meson-baryon pair, naturally leading to the suppression of charm-exchange processes². The tree-level

amplitudes of the theory are given by

$$V_{ij}^{IJSC}(\sqrt{s}) = D_{ij}^{IJSC} \frac{2\sqrt{s} - M_i - M_j}{4f_i f_j} \times \sqrt{\frac{E_i + M_i}{2M_i}} \sqrt{\frac{E_j + M_j}{2M_j}}, \quad (13)$$

where M_i and E_i denote the mass and CM energy of the baryon in channel i , respectively, f_i stands for the corresponding meson decay constant, and D^{IJSC} is a matrix of coefficients in the coupled-channel space for given isospin, spin, strangeness and charm numbers. Breaking of the SU(8) symmetry is taken into account by using physical hadron masses and meson decay constants in Eq. (13). The model is not complete in the analytic sense since no t - or u -channel mechanisms are explored; it is, however, a minimal extension of the SU(3) WT interaction with no additional free parameters which simultaneously implements the relevant symmetries of QCD in the light- and heavy-quark sectors.

The tree-level scattering amplitudes obtained from the previous approaches to the scattering of D/D^* mesons with light mesons and baryons are unitarized along the right-hand cut by solving the set of coupled-channel (on-shell) Bethe-Salpeter equations, $T = T + VGT$. Here T (V) stands for the unitarized (tree-level) amplitude with matrix element $T(V)_{ij}^{IJSC}$, where $i(j)$ labels the incident (outgoing) heavy-light meson or heavy-meson baryon state. G represents the two-particle propagator or loop function, which is regularized by subtractions or in dimensional regularization. The few parameters unconstrained in the heavy-light meson Lagrangian are fixed by the mass difference between the D and D_s mesons, and by the position and width of the $D_0^*(2400)$ resonance, which is dynamically generated by the unitarized interaction in the $I = 1/2$ $D\pi$ channel. We recall that the model for the meson-baryon interaction is parameter free, modulo regularization. The sub-threshold $\Lambda_c(2595)$ resonance is dynamically generated by the model, with a strong coupling to the DN and D^*N channels in $I = 0$ and a finite width from the $\Sigma_c\pi$ channel, which is open for decay. Several additional states in the $C = 1$ and $S = 0$ sector are generated by the interaction, some of which have been identified with experimental observations whereas others are genuine predictions that could be detected in the forthcoming CBM and PANDA experiments at GSI/FAIR [58].

A selection of the D and D^* cross sections off light mesons, nucleons and Δ baryons is shown in Fig. 10 for several physical (charge) states. The cross sections exhibit a remarkable isospin dependence, as expected, leading to rather different shapes (energy dependence). For example, the $D_0^*(2400)$ resonance is clearly visible in the $D^0\pi^+$ elastic reaction, which has a predominant $I = 1/2$ component. Conversely, the $D^0\pi^-$ elastic reaction is pure $I = 3/2$ and the cross section is not resonant in this case, whereas other processes exhibit deviations from the resonance profile due to the interference between

² This feature arises in other models based on meson exchange mechanisms due to the heavy mass of the charmed field and the large heavy-meson decay constants; note, however, that HQSS is not exactly fulfilled in most of these models [59].

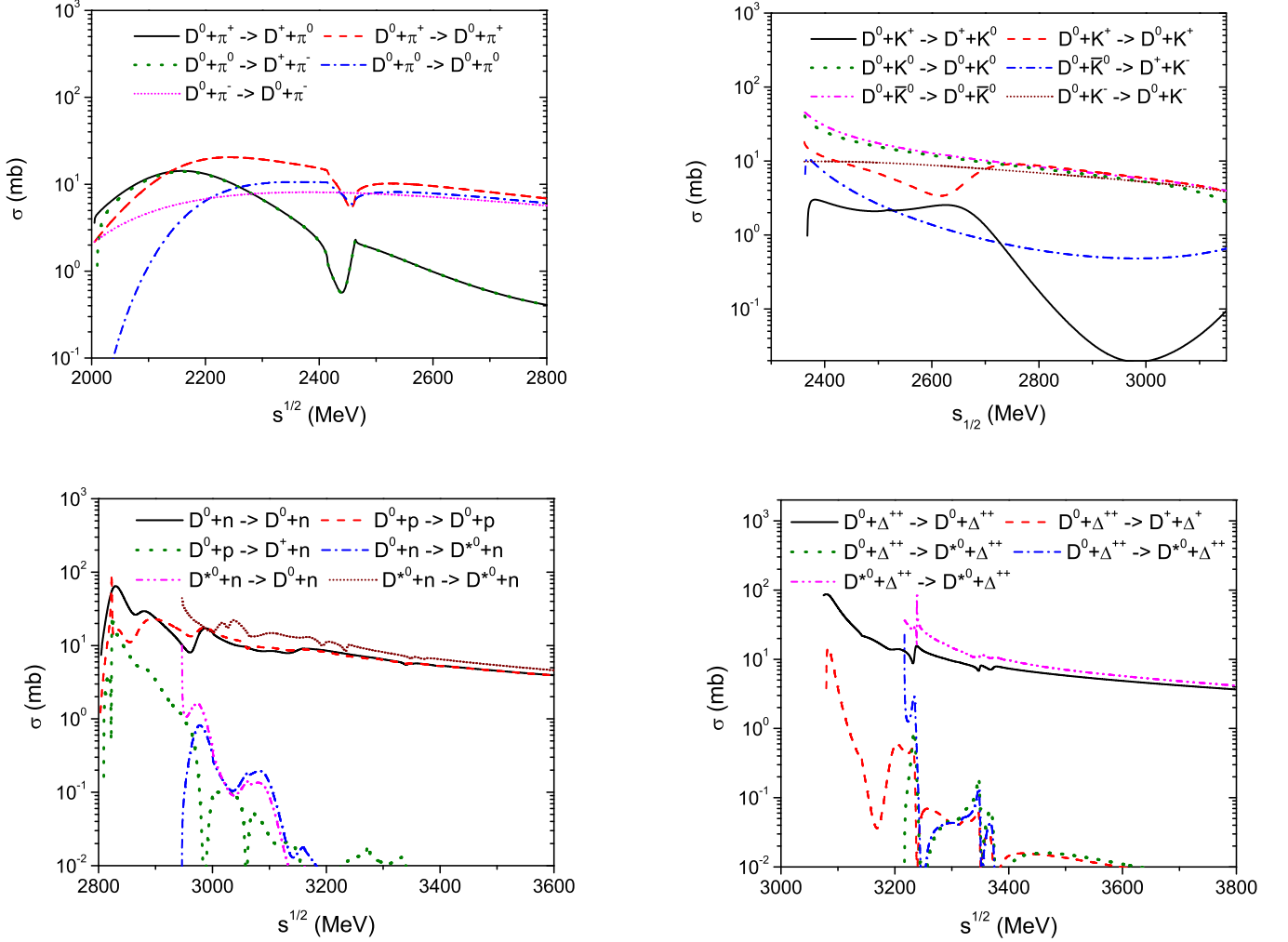


FIG. 10: (Color online) Several examples for the scattering cross sections of D and D^* mesons with light mesons and baryons.

the $I = 1/2, 3/2$ amplitudes. We note the dip caused by the opening of the $D\eta$ channel, which mixes with $D\pi$ only at NLO in the chiral Lagrangian. The DK cross sections present a characteristic monotonic fall due to the presence of the narrow $D_s^*(2317)$, which lies right below threshold energy (compare, e.g. with the cross section of the pure isovector D^0K^- , which is essentially flat). The isoscalar part of the DK amplitude contributes with a broad resonant state around 2700 MeV. Significantly, the vector partner $D_{s1}^*(2700)$ has been observed with a decay width of about 120 MeV. Similar cross sections are obtained for the D^* interaction as the underlying dynamics is identical at LO in the heavy-quark expansion, and the only differences are introduced by the slightly higher mass of the D^* (thus thresholds and resonances appear shifted by this amount). In addition to the subthreshold Λ_c and Σ_c states generated from the D and D^* interactions with baryons, the $D^{(*)}N$ and $D^{(*)}\Delta$ cross sections are populated by several resonances at higher energies,

with a remarkable isospin and coupled-channel dependence. In both cases the reactions with a strong isovector component seem to dominate over other processes. We also account explicitly for the cross sections of reactions with antinucleons, not shown in Fig. 10, which are obtained from the $\bar{D}N$ scattering amplitudes by charge conjugation. Finally, the cross sections for the scattering of D and D^* with the vector mesons from the octet (e.g. $D\rho$), out of the scope of the present model, have been set to an estimated value of 10 mb and independent of the collision energy.

Fig. 11 shows the distribution of D and D^* meson scatterings with pions and nucleons as a function of the invariant scattering energy \sqrt{s} in 0-10 % Au+Au central collisions. The total number of D and D^* meson scatterings with pions is about 49 and that with nucleons or antinucleons is ~ 6 . The numbers of D and D^* meson scatterings with all mesons and all baryons are, respectively, ~ 56 and ~ 10 . Considering that the number of D

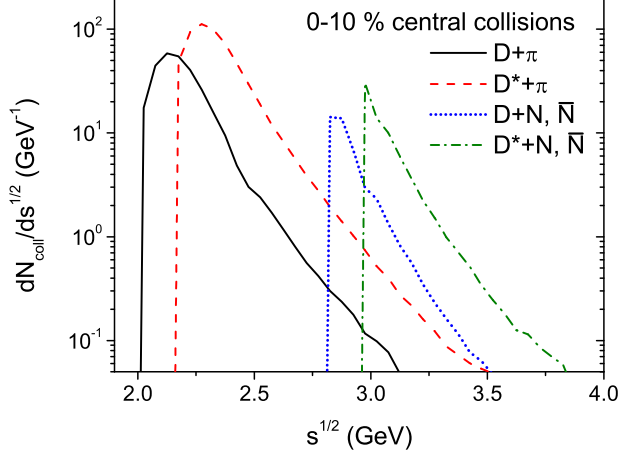


FIG. 11: (Color online) The distributions of D and D^* meson scattering with pions and nucleons as a function of the invariant scattering energy \sqrt{s} in 0-10 % Au+Au central collisions. See the legend for the individual channels.

and D^* mesons in 0-10 % central collisions is about 30, excluding D_s , D_s^* , Λ_c , and $\bar{\Lambda}_c$, each D or D^* meson experiences on average two scatterings with a hadron until it freezes out. Compared to Fig. 7, the number of scatterings decreases rapidly with increasing scattering energy. This is attributed to the decrease of hadronic cross sections beyond the resonance region, as shown in Fig. 10. Accordingly, hadronic interactions become ineffective for the energy loss of D and D^* mesons at high transverse momentum.

VII. RESULTS

The nuclear modification of D mesons is expressed in term of the ratio R_{AA} which is defined as

$$R_{AA}(p_T) \equiv \frac{dN_D^{\text{Au+Au}}/dp_T}{N_{\text{binary}}^{\text{Au+Au}} \times dN_D^{\text{p+p}}/dp_T}, \quad (14)$$

where $N_D^{\text{Au+Au}}$ and $N_D^{\text{p+p}}$ are, respectively, the number of D mesons produced in Au+Au collisions and that in p+p collisions, and $N_{\text{binary}}^{\text{Au+Au}}$ is the number of binary nucleon-nucleon collisions in Au+Au collision for the centrality class considered. If the matter produced in relativistic heavy-ion collisions does not modify the D meson production and propagation, the numerator of Eq. (14) should be equal to the denominator. Therefore, an R_{AA} smaller or larger than one implies that the nuclear matter suppresses or enhances D mesons, respectively.

In order to see the effect of partonic scattering, all hadronic scatterings of D mesons are switched off in Fig. 12. The dotted, dashed, solid, and dot-dashed lines in the figure show the R_{AA} of D^0 mesons in 0-10 % central Au+Au collisions with the cross sections for the partonic

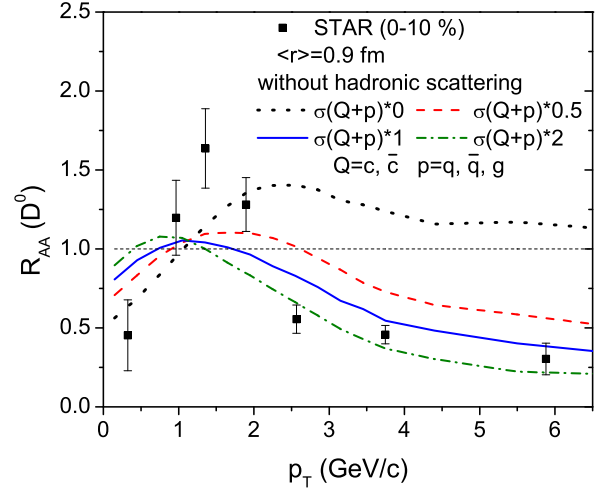
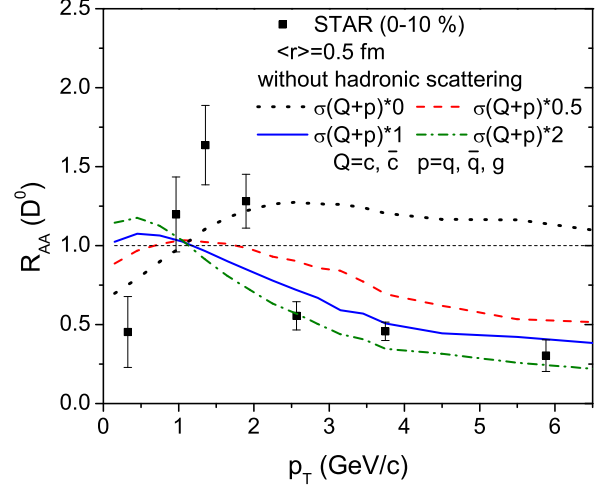


FIG. 12: (Color online) The R_{AA} of D^0 mesons without hadronic scattering in 0-10 % central Au+Au collisions at $\sqrt{s_{NN}}=200$ GeV for a radius of the D meson of 0.5 fm (upper) and of 0.9 fm (lower), which are compared with the experimental data from the STAR Collaboration [6]. The cross sections for charm-parton scattering are multiplied by factors of 0, 0.5, 1, and 2 for the dotted, dashed, solid, and dot-dashed lines, respectively.

scattering of charm being artificially multiplied by factors of 0, 0.5, 1, and 2, respectively. We stress that these multiplication factors are introduced in order to explore the impact of the partonic interaction strength on the shape of $R_{AA}(p_T)$. Note, however, that the default cross section (multiplication factor 1) is determined consistently on the basis of the DQPM couplings and propagators and thus has no free parameters. The fact that the $R_{AA}(p_T)$ is best described by the consistent cross sections (blue solid lines) points towards an experimental support of our approach. The black dotted line, where both partonic and hadronic scatterings are absent, shows that

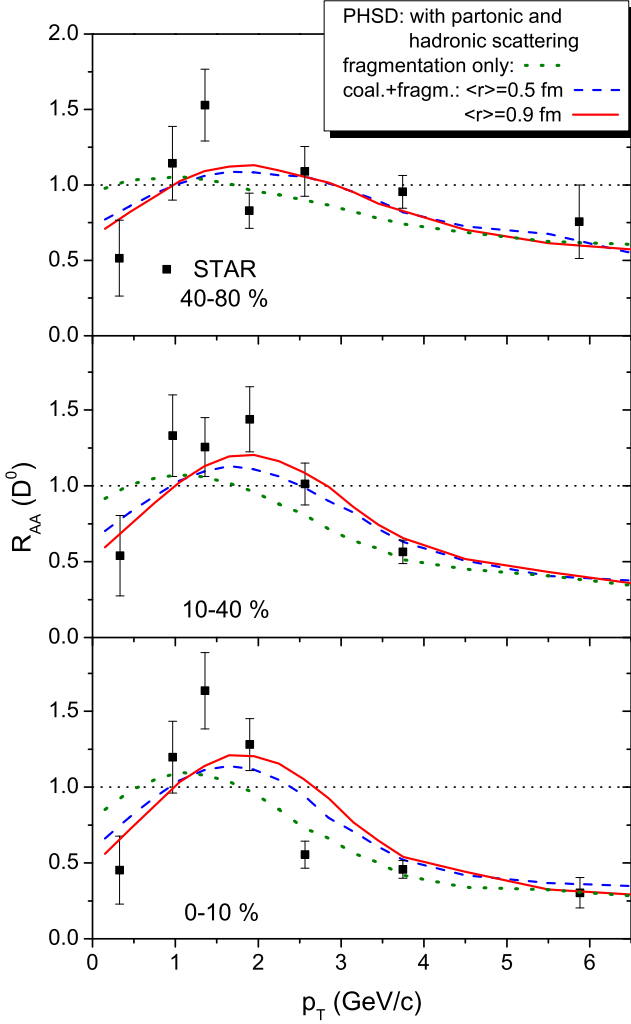


FIG. 13: (Color online) The R_{AA} of D^0 mesons in Au+Au collisions at $\sqrt{s_{NN}}=200$ GeV including partonic and hadronic scatterings for the D meson radius of 0.5 fm (dashed lines), of 0.9 fm (solid lines), and without coalescence, i.e. fragmentation only (dotted lines), which are compared with the experimental data from the STAR Collaboration [6].

R_{AA} approaches 1 at high p_T as it ought to be. However, the coalescence of charm quarks creates a peak in R_{AA} around $p_T = 2.5$ GeV/c. This peak does not show up in the PHSD calculations when discarding the dissolution of strings to partons. In this case the R_{AA} is unity. The peak emerges because the charm hadron gains transverse momentum in the coalescence which is absent in p+p collisions. The red dashed, blue solid, and green dot-dashed lines show that with increasing cross section for charm and parton scattering the charm quark loses more energy at high p_T . It is also seen that the energy loss of a charm or anticharm quark at high p_T can be dominantly attributed to the interaction with partons in the QGP. On the other hand, the R_{AA} at low p_T increases with

increasing scattering cross section. The reason is that a larger scattering cross section produces charm quarks closer to their thermal equilibrium distribution as shown in Fig. 8, which is enhanced at low p_T relative to the initial p_T distribution.

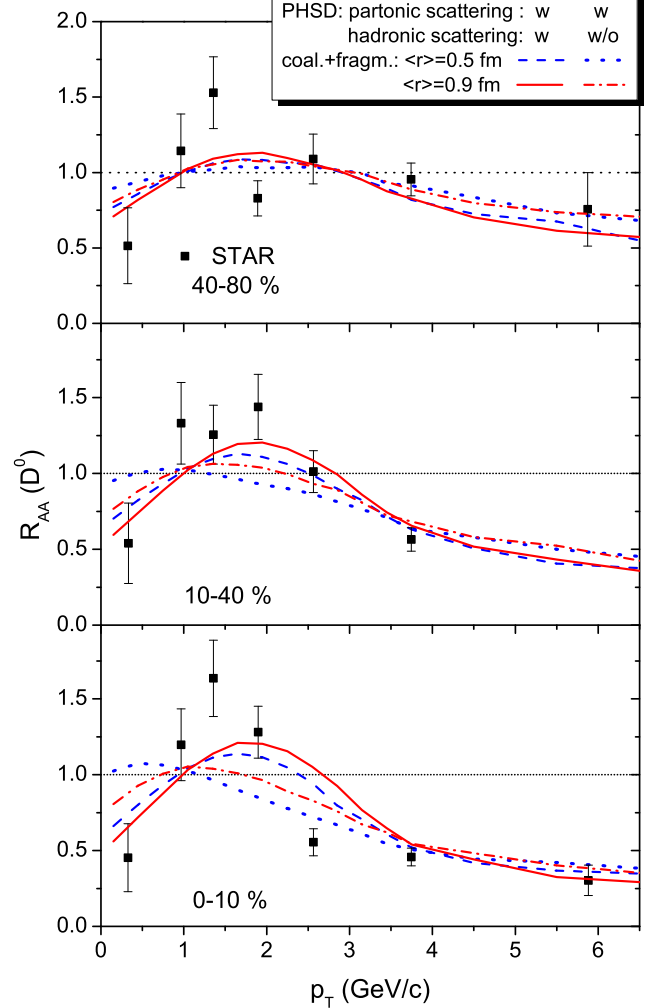


FIG. 14: (Color online) The R_{AA} of D^0 mesons including partonic scattering with (dashed and solid lines) and without hadronic scattering (dotted and dot-dashed lines) in Au+Au collisions at $\sqrt{s_{NN}}=200$ GeV for a D meson radius of 0.5 fm and of 0.9 fm. The experimental data are from the STAR Collaboration [6, 7].

In Fig. 13 we show the effect of the coalescence probability on the R_{AA} of D^0 mesons. The dashed and solid lines are, respectively, the R_{AA} for a D meson radius of 0.5 fm and of 0.9 fm as shown in Fig. 9. For the dotted lines, all charm and anticharm quarks are hadronized by fragmentation. It is seen that for the D meson radius of 0.9 fm more charm quarks are hadronized through coalescence and as a result the peak of R_{AA} is shifted to higher p_T . On the contrary, when all charm quarks are

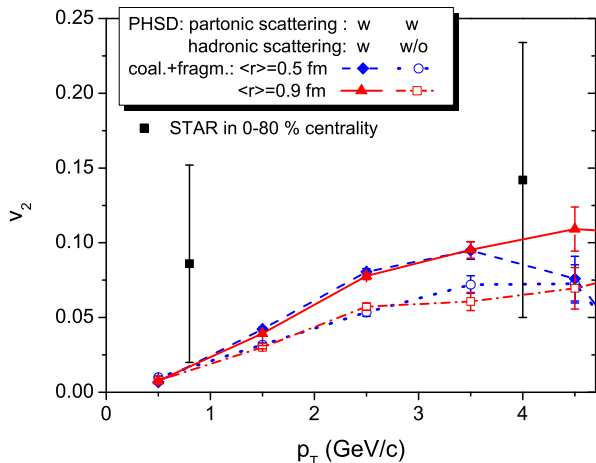


FIG. 15: (Color online) The elliptic flow v_2 of D^0 mesons including partonic scattering with (dashed and solid lines) and without hadronic scattering (dotted and dot-dashed lines) in Au+Au collisions at $\sqrt{s_{NN}}=200$ GeV for a D meson radius of 0.5 fm and of 0.9 fm. The experimental data are from the STAR Collaboration [6, 7].

hadronized through fragmentation, the peak is shifted to lower p_T .

Finally, Fig. 14 shows the R_{AA} and Fig. 15 the elliptic flow v_2 of D^0 mesons with and without hadronic scattering. We can see that the hadronic scattering plays an important role both in R_{AA} and the elliptic flow v_2 . It shifts the peak of R_{AA} to higher transverse momentum especially in central collisions and enhances the elliptic flow of final D mesons.

VIII. SUMMARY

We have studied charm production in relativistic heavy-ion collisions by using the Parton-Hadron-String Dynamics (PHSD) approach [27] where the initial charm quark pairs are produced in binary nucleon-nucleon collisions from the PYTHIA event generator [43] taking into account the smearing of the collision energy due to the Fermi motion of nucleons in the initial nuclei. The produced charm and anticharm quarks interact with the dressed quarks and gluons in the QGP which are described by the Dynamical Quasi-Particle Model [38] in PHSD. The interactions of the charm quarks with the QGP partons have been evaluated with the DQPM propagators and couplings consistently [33]. Furthermore, when extracting the spatial diffusion coefficient D_s from our cross sections (Fig. 6) as a function of the temperature we observe a minimum of D_s close to T_c which is in line with lattice data above T_c and hadronic many-body calculations below T_c .

We recall that the PHSD differs from conventional Boltzmann approaches incorporating on-shell scattering

with pQCD cross sections in a couple of essential aspects:

- i) it incorporates dynamical quasi-particles due to the finite width of the spectral functions;
- ii) it involves scalar mean-fields for the light partons that substantially drive the collective flow in the partonic phase and includes c -quark scattering with the QGP partons that transfers collective flow also to the charm quarks;
- iii) it is based on a realistic equation of state from lattice QCD and thus describes the speed of sound $c_s(T)$ reliably (without incorporating a first order phase transition);
- iv) the hadronization of 'bulk' partons is described by the fusion of off-shell partons to off-shell hadronic states (resonances or strings) and does not violate the second law of thermodynamics;
- v) all conservation laws (energy-momentum, flavor currents etc.) are fulfilled in the hadronization (contrary to some coalescence models);
- vi) the effective partonic cross sections no longer are given by pQCD and are evaluated within the DQPM in a consistent fashion and probed by transport coefficients (correlators) in thermodynamic equilibrium (shear- and bulk viscosity, electric conductivity, magnetic susceptibility, spatial charm diffusion coefficient etc. [35, 40, 41]).

We have found that the interaction with the dynamical partons of the QGP softens the p_T spectrum of charm and anticharm quarks but does not lead to a full thermalization for transverse momenta $p_T > 2$ GeV/c. The charm and anticharm quarks, furthermore, are hadronized to D mesons either through the coalescence with a light quark or antiquark or through the fragmentation by emitting soft 'perturbative' gluons. Since the hadronization through coalescence is absent in p+p collisions, it can be interpreted as a nuclear matter effect on the D meson production in relativistic heavy-ion collisions. In the coalescence mechanism the charm or anticharm quark gains momentum by fusing with a light quark or antiquark while it loses momentum in the fragmentation process (as in p+p reactions). This partly contributes to the large R_{AA} of D mesons between 1 and 2 GeV/c of transverse momentum. Finally, the formed D mesons interact with hadrons by using the cross sections calculated in an effective lagrangian approach with heavy quark spin-symmetry [32], which is state-of-the art. We have found that the contribution from hadronic scattering both to the R_{AA} and to the elliptic flow of D mesons is appreciable, especially in central collisions, and produces additional elliptic flow v_2 .

Since the PHSD results reproduce the experimental data from the STAR Collaboration without radiative energy loss in the p_T range considered, we conclude that collisional energy loss is dominant at least up to $p_T = 6$ GeV/c in relativistic heavy-ion collisions. In our approach this is essentially due to the infrared enhanced coupling $\alpha_s(T)$ in the DQPM leading to large scattering cross sections of charm quarks with partons at temperatures close to T_c and to rather massive gluons in the partonic bulk matter. It will be of future interest to

perform a similar study at LHC energies for Pb+Pb reactions since here a significantly larger p_T range can be addressed and the effect of gluon bremsstrahlung might become important again [48]. Furthermore, angular correlations between pairs of $D \bar{D}$ mesons are expected to provide further valuable information.

Acknowledgements

The authors acknowledge inspiring discussions with J. Aichelin, P. B. Gossiaux, C. M. Ko, O. Linnyk, R.

Marty, V. Ozvenchuk, and R. Vogt. This work was supported by DFG under contract BR 4000/3-1, and by the LOEWE center "HIC for FAIR". JMTR is supported by the Program TOGETHER from Region Pays de la Loire and the European I3-Hadron Physics program. LT acknowledges support from the Ramon y Cajal Research Programme and contracts FPA2010-16963 and FPA2013-43425-P from Ministerio de Ciencia e Innovación, as well as from FP7-PEOPLE-2011-CIG under Contract No. PCIG09-GA-2011-291679. The computational resources have been provided by the LOEWE-CSC.

-
- [1] Z. Fodor and S. D. Katz, JHEP **0203**, 014 (2002); Z. Fodor, S. D. Katz, and K.K. Szabo, Phys. Lett. B **568**, 23 (2003).
- [2] Proceedings of Quark Matter-2014, Nucl. Phys. A **931**, 1 (2014).
- [3] M. Cacciari, P. Nason and R. Vogt, Phys. Rev. Lett. **95**, 122001 (2005).
- [4] A. Adare et al. (PHENIX Collaboration), Phys. Rev. Lett. **98**, 172301 (2007).
- [5] B. I. Abelev et al. [STAR Collaboration], Phys. Rev. Lett. **98**, 192301 (2007) [Erratum-ibid. **106**, 159902 (2011)].
- [6] L. Adamczyk et al. [STAR Collaboration], Phys. Rev. Lett. **113**, 142301 (2014).
- [7] D. Tlusty [STAR Collaboration], Nucl. Phys. A **904-905**, 639c (2013).
- [8] B. Abelev et al. [ALICE Collaboration], J. High Energy Phys. **09**, 112 (2012); S. Sakai et al. Nucl. Phys. A **904-905**, 661c (2013).
- [9] M. Golam Mustafa, D. Pal and D. Kumar Srivastava, Phys. Rev. C **57**, 889 (1998) [Erratum-ibid. C **57**, 3499 (1998)].
- [10] G. D. Moore and D. Teaney, Phys. Rev. C **71**, 064904 (2005).
- [11] B. Zhang, L. W. Chen and C. M. Ko, Phys. Rev. C **72**, 024906 (2005).
- [12] D. Molnar, Eur. Phys. J. C **49**, 181 (2007).
- [13] H. van Hees, V. Greco and R. Rapp, Phys. Rev. C **73**, 034913 (2006).
- [14] P. B. Gossiaux and J. Aichelin, Phys. Rev. C **78** 014904, (2008); P. B. Gossiaux, R. Bierkandt and J. Aichelin, Phys. Rev. C **79** 044906, (2009); J. Aichelin, P. B. Gossiaux and T. Gousset, Phys. Rev. D **89** 074018, (2014).
- [15] M. Nahrgang, J. Aichelin, S. Bass, P. B. Gossiaux and K. Werner, Phys. Rev. C **91** (2015) 1, 014904.
- [16] V. Ozvenchuk, J. M. Torres-Rincon, P. B. Gossiaux, L. Tolos and J. Aichelin, Phys. Rev. C **90**, 054909 (2014).
- [17] S. Cao, G. Y. Qin and S. A. Bass, Phys. Rev. C **88**, 044907 (2013).
- [18] W. M. Alberico, A. Beraudo, A. De Pace, A. Molinari, M. Monteno, M. Nardi and F. Prino, Eur. Phys. J. C **71**, 1666 (2011); *ibid* **73**, 2481 (2013).
- [19] R. Sharma, I. Vitev and B. W. Zhang, Phys. Rev. C **80**, 054902 (2009).
- [20] M. He, R. J. Fries and R. Rapp, Phys. Rev. C **86**, 014903 (2012); Phys. Rev. Lett. **110**, 112301 (2013).
- [21] Y. Akamatsu, T. Hatsuda and T. Hirano, Phys. Rev. C **79**, 054907 (2009).
- [22] J. Uphoff, O. Fochler, Z. Xu and C. Greiner, Nucl. Phys. A **910-911**, 401 (2013); *ibid* **931** (2014) 535.
- [23] T. Lang, H. van Hees, J. Steinheimer and M. Bleicher, arXiv:1208.1643 [hep-ph].
- [24] S. K. Das, F. Scardina, S. Plumari and V. Greco, Phys. Rev. C **90**, 044901 (2014).
- [25] S. K. Das, F. Scardina, S. Plumari and V. Greco, arXiv:1502.03757 [nucl-th].
- [26] W. Cassing and E.L. Bratkovskaya, Nucl. Phys. A **831**, 215 (2009).
- [27] E. L. Bratkovskaya, W. Cassing, V. P. Konchakovski and O. Linnyk, Nucl. Phys. A **856**, 162 (2011).
- [28] V. P. Konchakovski et al., J. Phys. G **42**, 055106 (2015); J. Phys. G **41**, 105004 (2014); Phys. Rev. C **90**, 014903 (2014); Phys. Rev. C **85**, 044922 (2012); Phys. Rev. C **85**, 011902 (2012).
- [29] O. Linnyk et al., Phys. Rev. C **89**, 034908 (2014); Phys. Rev. C **88**, 034904 (2013); Phys. Rev. C **87**, 014905 (2013); Phys. Rev. C **85**, 024910 (2012); Phys. Rev. C **84**, 054917 (2011); Nucl. Phys. A **855**, 273 (2011).
- [30] W. Cassing and E. L. Bratkovskaya, Phys. Rep. **308**, 65 (1999); W. Cassing, E.L. Bratkovskaya, and S. Juchem, Nucl. Phys. A **674**, 249 (2000).
- [31] O. Linnyk, E.L. Bratkovskaya, and W. Cassing, Int. J. Mod. Phys. E **17**, 1367 (2008).
- [32] L. Tolos and J. M. Torres-Rincon, Phys. Rev. D **88**, 074019 (2013).
- [33] H. Berrehrhah, E. Bratkovskaya, W. Cassing, P. B. Gossiaux, J. Aichelin and M. Bleicher, Phys. Rev. C **89**, 054901 (2014).
- [34] H. Berrehrhah, P. B. Gossiaux, J. Aichelin, W. Cassing and E. Bratkovskaya, Phys. Rev. C **90**, 064906 (2014).
- [35] H. Berrehrhah, P.B. Gossiaux, J. Aichelin, W. Cassing, J.M. Torres-Rincon, and E. Bratkovskaya, Phys. Rev. C **90**, 051901 (2014).
- [36] L. P. Kadanoff and G. Baym, *Quantum Statistical Mechanics*, Benjamin, New York, 1962.
- [37] S. Juchem, W. Cassing, and C. Greiner, Phys. Rev. D **69**, 025006 (2004); Nucl. Phys. A **743**, 92 (2004).
- [38] W. Cassing, Eur. Phys. J. ST **168**, 3 (2009); Nucl. Phys. A **795**, 70 (2007).
- [39] V. Ozvenchuk, O. Linnyk, M.I. Gorenstein, E.L. Bratkovskaya, and W. Cassing, Phys. Rev. C **87**, 024901 (2013).
- [40] V. Ozvenchuk, O. Linnyk, M.I. Gorenstein, E.L.

- Bratkovskaya and W. Cassing, Phys.Rev. C **87**, 064903 (2013). Rev. C **87**, 064903 (2013).
- [41] W. Cassing, O. Linnyk, T. Steinert, and V. Ozvenchuk, Phys. Rev. Lett. **110**, 182301 (2013); T. Steinert and W. Cassing, Phys. Rev. C **89**, 035203 (2014).
- [42] B. Andersson, G. Gustafson, and H. Pi, Z. Phys. C **57**, 485 (1993).
- [43] T. Sjostrand, S. Mrenna and P. Z. Skands, JHEP **0605**, 026 (2006).
- [44] L. Adamczyk *et al.* [STAR Collaboration], Phys. Rev. D **86**, 072013 (2012).
- [45] C. Amsler *et al.* [Particle Data Group Collaboration], Phys. Lett. B **667**, 1 (2008).
- [46] C. Peterson, D. Schlatter, I. Schmitt and P. M. Zerwas, Phys. Rev. D **27**, 105 (1983).
- [47] Z. Conesa del Valle [ALICE Collaboration], AIP Conf. Proc. **1441**, 886 (2012).
- [48] M. Younus, C. E. Coleman-Smith, S. A. Bass and D. K. Srivastava, Phys. Rev. C **91**, 024912 (2015).
- [49] D. Banerjee *et al.*, Phys. Rev. D **85**, 014510 (2012).
- [50] U. W. Heinz, hep-ph/0407360.
- [51] T. Song, W. Park and S. H. Lee, Phys. Rev. C **84**, 054903 (2011).
- [52] K. A. Olive *et al.* [Particle Data Group Collaboration], Chin. Phys. C **38**, 090001 (2014).
- [53] Y. Oh, C. M. Ko, S. H. Lee and S. Yasui, Phys. Rev. C **79**, 044905 (2009).
- [54] L. M. Abreu, D. Cabrera, F. J. Llanes-Estrada and J. M. Torres-Rincon, Annals Phys. **326**, 2737 (2011).
- [55] L. M. Abreu, D. Cabrera and J. M. Torres-Rincon, Phys. Rev. D **87**, 034019 (2013).
- [56] J. M. Torres-Rincon, L. Tolos and O. Romanets, Phys. Rev. D **89**, 074042 (2014).
- [57] C. Garcia-Recio, V. K. Magas, T. Mizutani, J. Nieves, A. Ramos, L. L. Salcedo and L. Tolos, Phys. Rev. D **79**, 054004 (2009).
- [58] O. Romanets, L. Tolos, C. Garcia-Recio, J. Nieves, L. L. Salcedo and R. G. E. Timmermans, Phys. Rev. D **85**, 114032 (2012).
- [59] C. Garcia-Recio, J. Nieves, O. Romanets, L. L. Salcedo and L. Tolos, Phys. Rev. D **87**, 074034 (2013).
- [60] L. Tolos, Int. J. Mod. Phys. E **22**, 1330027 (2013).
- [61] D. Gamermann, C. Garcia-Recio, J. Nieves and L. L. Salcedo, Phys. Rev. D **84**, 056017 (2011).